JACS
JOURNAL OF THE AMERICAN CHEMICAL SOCIETY
Article
pubs.acs.org/JACS

Hollow and Cage-Bell Structured Nanomaterials of Noble Metals

Hui Liu,[†] Jianglan Qu,[†] Yunfa Chen,[†] Jianqiang Li,[†] Feng Ye,[†] Jim Yang Lee,*[,‡] and Jun Yang*[,†,§]

[†]State Key Laboratory of Multiphase Complex Systems, Institute of Process Engineering, Chinese Academy of Sciences, Beijing, China 100190

[‡]Department of Chemical and Biomolecular Engineering, National University of Singapore, 10 Kent Ridge Crescent, Singapore 119260

[§]Institure of Bioengineering and Nanotechnology, 31 Biopolis Way, The Nanos, Singapore 138669

Supporting Information

ABSTRACT: Mastery of the structure of nanomaterials enables control of their properties to enhance their performance for a given application. Herein we demonstrate the synthesis of metal nanomaterials with hollow interiors or cage-bell structures based on the inside-out diffusion of Ag in core−shell structured nanoparticles. It begins with the synthesis of core−shell Ag−M or core−shell−shell M_A−Ag−M_B nanoparticles in an organic solvent. Ag is then extracted from the core or the inner shell by bis(p-sulfonatophenyl)phenylphosphane, which binds strongly with Ag(I)/Ag(0) to allow the complete removal of Ag in 24−48 h, leaving behind an organosol of hollow or cage-bell structured metal nanomaterials. Because of their relatively lower densities, which usually translate to a higher surface area than their solid counterparts, the hollow and cage-bell structured metal nanomaterials are especially relevant to catalysis. For example, cage-bell structured Pt−Ru nanoparticles were found to display outstanding methanol tolerance for the cathode reaction of direct methanol fuel cells (DMFCs) as a result of the differential diffusion of methanol and oxygen in the cage-bell structure.

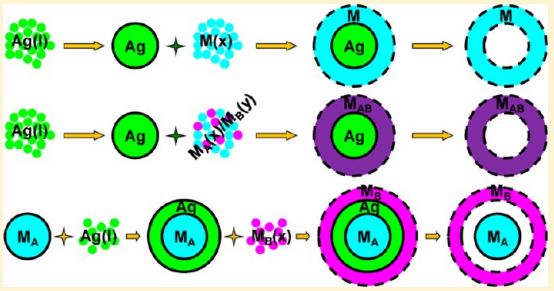

1. INTRODUCTION

Noble metal nanomaterials with customizable internal structures and shell compositions have garnered sustained research interest due to their immense potential for catalysis.[1−3] For instance, Pd nanoparticles with a hollow interior exhibit good catalytic activity in Suzuki cross-coupling reactions and can be reused seven times without the loss of catalytic activity.[1] Liang and co-workers showed that Pt hollow nanospheres are twice as active as solid Pt nanoparticles of roughly the same size for methanol oxidation.[4] The increase in activity could be attributed mainly to the larger surface area of the hollow structure, where the porous shell allows the internal surface of the catalyst to be accessible to the reactants. The continuing research efforts in this area have also given rise to the recent possibility of creating hybrids of core−shell and hollow structures, or a new class of core−shell structures with a distinctive core-void-shell configuration, which are called cage-bell, yolk-shell, or rattle-type structures. With the unique properties of a movable core, interior void spaces, and controlled porosity and composition of the shell, cage-bell structured (CBS) nanomaterials have great potential for a diverse range of applications, such as nanoreactors,[5−7] drug delivery systems,[8−10] lithium-ion batteries,[11−15] photocatalysis,[16] and photonics.[17] For example, polymeric hollow spheres with a movable Au nanoparticle core have been synthesized, which allow the optical sensing of chemicals diffused into the cavity.[18] Most recently, Fan and co-workers developed a photocatalytic approach using densely packed optically active porpyrins to template the synthesis of well-defined hollow Pt nanostructures which were excellent catalyst for the methanol oxidation reaction.[19] The authors also demonstrated reusability of the template by an acid−base treatment. A general strategy for the fabrication of hollow or CBS structures is template-assisted selective etching of core−shell particles. The core particle in this case is overlaid with a single or double shell of a different material. The core or the inner shell is then selectively removed by calcination or with a solvent. Over the past 20 years, various methods based on sacrificial templates of polymer and inorganic spheres,[20−26] liquid droplets,[27] vesicles,[28−30] and microemulsion droplets,[31−33] have been developed for the synthesis of hollow and CBS nanomaterials, and were reviewed recently by the Lou, Jiang, and Lu groups.[34−36] These preparative methods are however system specific, more successful for metal oxides than for noble metals. Specific methods based on other principles such as galvanic replacement,[37,38] Kirkendall effect,[8,39] Ostwald ripening,[40,41] and layer-by-layer assembly[23,42] have also been used for the synthesis of hollow or cage-bell nanomaterials. These methods are only applicable to a small number of metals (mostly Au and Pt) and there are significant limitations. For example, the core and the shell of cage-bell nanostructures prepared this way are usually made of the same material, and there is no effective control of the shell thickness and shell

Received: March 15, 2012

   dx.doi.org/10.1021/ja302518n | J. Am. Chem. Soc. XXXX, XXX, XXX−XXX

structure.[43,44] In summary, a general approach to rationally fabricate hollow and cage-bell structures for a sufficiently wide spectrum of noble metals is still lacking today and it poses significant challenges.

Herein, we report a facile generic approach, which is based on the inside-out diffusion of Ag in core−shell structures, for the fabrication of hollow or cage-bell noble metal nanomaterials. In this strategy, core−shell Ag−M nanoparticles or core−shell−shell M_A−Ag−M_B nanoparticles are first prepared in an organic solvent, followed by the removal of Ag from the core or the inner shell with bis(*p*-sulfonatophenyl)phenylphosphane dihydrate dipotassium salt (BSPP), which binds strongly with Ag(I)/Ag(0) to promote the inside-out diffusion of Ag in the core−shell structure, which is typically completed in 24−48 h. In this report, the preparation of monometallic nanoparticles with a hollow interior will be demonstrated first, followed by the preparation of hollow nanoparticles with a bimetallic or trimetallic alloy shell, and finally CBS metal nanomaterials with different core and shell compositions. The hollow and CBS nanoparticles prepared as such have relatively lower densities, which usually translate to a higher surface area than their solid counterparts; hence, a higher degree of metal utilization (for example, in catalysis) can be expected. In particular, CBS Pt−Ru nanoparticles were found to exhibit outstanding methanol tolerance for the cathode reaction of the direct methanol fuel cell (DMFC). This may be attributed to the difference in the diffusion of methanol and oxygen through the shell of the CBS nanoparticles. Hence, a diffusion-limited design, rather than the intrinsic properties of the catalytic metals, may be used to deliver the desired catalyst selectivity for the mitigation of the methanol crossover problem in DMFCs.

2. EXPERIMENTAL SECTION

2.1. Materials and Common Procedures. Ruthenium(III) chloride ($RuCl_3$, Ru content 45−55%), rhodium(III) chloride ($RhCl_3$, 98%), palladium(II) chloride ($PdCl_2$, 99%), silver nitrate ($AgNO_3$, 99%), osmium(III) chloride ($OsCl_3$, 99.9%), iridium(IV) chloride ($IrCl_4$, 98%) potassium tetrachloroplatinate(II) (K_2PtCl_4, 98%), gold(III) chloride ($AuCl_3$, 99%), oleylamine (70%, technical grade), sodium sulfide nonahydrate ($Na_2S{\cdot}9H_2O$, ≥98%), selenide powder (Se, ≥99.5%), tellurium powder (Te, 99.8%), sodium borohydride ($NaBH_4$, 98%), sodium citrate dehydrate ($HOC(COONa)(CH_2COONa)_2 \cdot 2H_2O$, ≥99%), dodecylamine (DDA, 98%), aqueous $HClO_4$ solution (70%, ACS reagent), and Nafion 117 solution (5% in a mixture of lower aliphatic alcohols and water) from Sigma-Aldrich; methanol (99%) and ethanol (99.5%) from Merck; toluene (99.5%) from J. T. Baker; bis(*p*-sulfonatophenyl)phenylphosphane dihydrate dipotassium salt (BSPP, 97%) from Strem Chemicals; hexadecyltrimethylammonium bromide (CTAB, 98%) from Lancaster; and Vulcan XC-72 carbon powders (XC-72C, BET surface area = 250 m^2/g and average particle size = 40−50 nm) from Cabot were used as received. All glassware and Teflon-coated magnetic stir bars were cleaned with *aqua regia*, followed by copious rinsing with deionized water before drying in an oven.

2.2. Synthesis of Ag, Au, and Pt Nanoparticle Seeds. In a typical synthesis of Ag or Au nanoparticles, 85 mg of $AgNO_3$ (or 80 mg of $AuCl_3$) was dissolved in 20 mL of oleylamine placed in a three-necked flask equipped with a condenser and stir bar. The solution was heated to 150 °C under flowing Ar or N_2 and kept at this condition for 1 h for the reduction of Ag^+ (or Au^{3+}) ions by oleylamine, which also served as the capping agent. No other reducing agent and stabilizer were used to form the Ag or Au nanoparticles (Supporting Information Figure S1a−d). For the synthesis of Pt nanoparticles, 70 mg of K_2PtCl_4 and 2 mg of $AgNO_3$ were added to 20 mL of oleylamine. A small amount of $AgNO_3$ was needed to promote the formation of spherical Pt nanoparticles (Supporting Information Figure S1e,f). In the absence of Ag, Pt nanotetrapods would be formed instead (Supporting Information Figure S2). The mixture was then heated and kept at 160 °C for 1 h with stirring under flowing Ar or N_2. After reaction, the Ag, Au, and Pt nanoparticles were purified by precipitation with methanol, followed by centrifugation and washing with methanol, and then redispersed in 20 mL of toluene.

2.3. Synthesis of Core−Shell Ag−M (M = Ru, Rh, Pd, Pt, Os, Ir, PtRu, PtRh, PtOs, PtRuOS, or PtRhOs) Nanoparticles. For the synthesis of core−shell nanoparticles with a Ag core and a monometallic shell, 85 mg of $AgNO_3$ was added to 20 mL of oleylamine in a three-necked flask fitted with a condenser and a stir bar. The solution was heated and kept at 150 °C under flowing Ar or N_2 for 1 h for the reduction of Ag^+ by oleylamine. Then, 104 mg of $RuCl_3$, or 105 mg of $RhCl_3$, 88 mg of $PdCl_2$, 148 mg of $OsCl_3$, 220 mg of $IrCl_4$, 208 mg of K_2PtCl_4 was added swiftly, followed by heating and keeping at the target temperature (160 °C for Pd and Pt, 250 °C for Rh, 320 °C for Ru, Os, and Ir) for 1 h under flowing Ar or N_2 for the reduction of the shell metal precursor. After reaction, the core−shell Ag−M nanoparticles were purified by precipitation with methanol, centrifugation, washing with methanol, and redispersed in 20 mL of toluene.

For the synthesis of core−shell nanoparticles with a Ag core and an alloy shell, 85 mg of $AgNO_3$ was added to 20 mL of oleylamine in a three-necked flask fitted with a condenser and stir bar. The solution was heated to and maintained at 150 °C under flowing Ar or N_2 for 1 h for the reduction of Ag^+ by oleylamine. Then, 104 mg K_2PtCl_4/52 mg $RuCl_3$, or 104 mg K_2PtCl_4/52 mg $RhCl_3$, 104 mg K_2PtCl_4/74 mg $OsCl_3$, 70 mg K_2PtCl_4/35 mg $RuCl_3$/50 mg $OsCl_3$, 70 mg K_2PtCl_4/35 mg $RhCl_3$/50 mg $OsCl_3$ was added swiftly, followed by heating and keeping at the target temperature (250 °C for PtRh, 320 °C for PtRu, PtOs, PtRuOs, and PtRhOs) for 1 h under flowing Ar or N_2 for the reduction of the shell metal precursors. After reaction, the core−shell nanoparticles were purified by precipitation with methanol, centrifugation, washing with methanol, and redispersed in 20 mL of toluene.

2.4. Inside-out Diffusion of Ag in Core−Shell Ag−M Nanoparticles. Typically, the inside-out diffusion of Ag in core−shell Ag−Ru nanoparticles, core−shell Ag−Rh nanoparticles, and core−shell Ag−Pt nanoparticles was observable by transmission electron microscopy (TEM) after aging the core−shell nanoparticles in toluene at room temperature for 6, 8, and 7 months, respectively.

2.5. Synthesis of Hollow Metal Nanoparticles. For the syntheses of hollow metal nanoparticle based on the inside-out diffusion of Ag in core−shell nanoparticles, 4 mL of core−shell Ag−M nanoparticle solution was diluted with toluene to 100 mL. An aqueous BSPP solution was prepared by dissolving 500 mg of BSPP in 100 mL of water. The diluted core−shell Ag−M nanoparticles in toluene and the aqueous solution of BSPP were then mixed together. The molar ratio of BSPP/Ag in the mixture was calculated to be ∼10/1 (this ratio was also used in subsequent synthesis of cage-bell structured metal nanomaterials). The mixture was aged for 48 h under vigorous stirring at room temperature to remove Ag from the core−shell Ag−M nanoparticles. The mixture was left to stand, and the upper toluene phase was collected (nominally 0.5 mM of Ru, Rh, Os, Ir, or Pt; 0.25 mM of alloy PtRu, PtRh, or PtOs; 0.17 mM of alloy PtRuOs, or PtRhOs).

2.6. Synthesis of Ag_2X (X = S, Se, or Te) Nanoparticles. For the synthesis of Ag_2S nanocrystals, 1 mL of 50 mM aqueous solution of Na_2S was added swiftly to 50 mL of any of the aqueous phases obtained in section 2.5, which contained the complex formed by BSPP and Ag^I ions. The mixture was stirred for 1 h at room temperature. The color of the mixture turned brown from colorless, indicating the formation of Ag_2S hydrosol.

For the synthesis of Ag_2Se or Ag_2Te nanocrystals, 1 mL of 50 mM aqueous solution of Na_2Se or Na_2Te (prepared by reacting 79 mg of Se or 127 mg of Te powder with 38 mg of $NaBH_4$ in 20 mL of water) was added swiftly to 50 mL of any of the aqueous phases obtained in section 2.5. The mixture was heated to 80 °C and kept at this temperature with stirring for 1 h to form the Ag_2Se or Ag_2Te hydrosol.

The sulfonic groups of BSPP imparted negative charges to the Ag_2X (X = S, Se, or Te) nanocrystals, allowing us to manipulate the solubility of the Ag_2X nanocrystals in an organic phase using electrostatic interactions. The Ag_2X hydrosol was mixed with 50 mL of toluene solution of CTAB (100 mM) and the mixture was stirred for 3 min. CTAB/BSPP-stabilized Ag_2X nanocrystals were extracted to the toluene

dx.doi.org/10.1021/ja302518n | J. Am. Chem. Soc. XXXX, XXX, XXX−XXX

layer rapidly, leaving behind a colorless aqueous solution. The ion pair formation on the Ag_2X nanocrystals surface was induced by the electrostatic interaction between the negatively charged sulfonic anions on the surface of Ag_2X nanocrystals and the incoming ligand, hexadecyltrimethylammonium cations.

2.7. Synthesis of Core−Shell−shell M_A−Ag−M_B (M_A = Au or Pt; M_B = Ru, Os, Ir, Pt, or PtRh) Nanoparticles. For the synthesis of core−shell−shell Au−Ag−M_B (M_B = Os, Ir, or Pt) nanoparticles, 80 mg of $AuCl_3$ was dissolved in 20 mL of oleylamine in a three-necked flask fitted with a condenser and stir bar. The solution was heated to and maintained at 150 °C under flowing Ar or N_2 for 1 h for the reduction of Au^{3+} ions by oleylamine. Then, 85 mg of $AgNO_3$ was added swiftly and the reaction mixture was kept at 150 °C under flowing Ar or N_2 for another hour for the growth of Ag on the existing Au seeds. Then, 148 mg of $OsCl_3$, 220 mg of $IrCl_4$, or 208 mg of K_2PtCl_4 was added swiftly, followed by heating to and keeping at the target temperature (320 °C for Os and Ir, 160 °C for Pt) for 1 h under flowing Ar or N_2 for the reduction of the metal precursors in the presence of previously formed core−shell Au−Ag nanoparticles. After the reaction, the core−shell−shell Au−Ag−M_B nanoparticles were purified by precipitation with methanol, centrifugation, washing with methanol, and redispersed in 20 mL of toluene.

For the synthesis of core−shell−shell Pt−Ag−M_B (M_B = Ru, Os, Ir, Pt, or PtRh) nanoparticles, 70 mg of K_2PtCl_4 and 2 mg of $AgNO_3$ were added to 20 mL of oleylamine. The mixture was heated to and maintained at 160 °C for 1 h under flowing Ar or N_2 and stirring to prepare the Pt seeds. Then, 85 mg of $AgNO_3$ was added swiftly and the temperature of the reaction mixture was lowered to 150 °C and maintained at this temperature under flowing Ar or N_2 for another hour for the growth of Ag on existing Pt seeds. Then, 104 mg of $RuCl_3$, 148 mg of $OsCl_3$, 220 mg of $IrCl_4$, 208 mg of K_2PtCl_4, or 104 mg of K_2PtCl_4/52 mg of $RhCl_3$ was added swiftly, followed by heating and keeping the reaction mixture at the target temperature (320 °C for Ru, Os, and Ir; 160 °C for Pt, 250 °C for PtRh) for 1 h under flowing Ar or N_2 for the reduction of the metal precursors in the presence of previously formed core−shell Pt−Ag nanoparticles. After the reaction, these core−shell−shell Pt−Ag−M_B nanoparticles were purified by precipitation with methanol, centrifugation, washing with methanol, and redispersed in 20 mL of toluene.

2.8. Synthesis of Cage-Bell Structured (CBS) Metal Nanoparticles. For the syntheses of CBS metal nanomaterials based on the inside-out diffusion of Ag in core−shell nanoparticles, 4 mL of core−shell−shell M_A−Ag−M_B nanoparticle solution was diluted with toluene to 100 mL. An aqueous BSPP solution was prepared by dissolving 500 mg of BSPP in 100 mL of water. The diluted core−shell−shell M_A−Ag−M_B nanoparticles in toluene and the BSPP aqueous solution were then mixed together. The mixture was aged for 48 h under vigorous stirring at room temperature. The mixture was left to stand, and the upper toluene phase was collected.

2.9. Characterizations. TEM, high-resolution TEM (HRTEM), and high-angle annular dark-field scanning TEM (HAADF-STEM) were performed on a FEI Tecnai G^2 F20 electron microscope operating at 200 kV with a supplied software for automated electron tomography. For the TEM measurements, a drop of the nanoparticle solution was dispensed onto a 3-mm carbon-coated copper grid. Excess solution was removed by an absorbent paper, and the sample was dried under vacuum at room temperature. Average particle size and particle size distribution were sampled from a few randomly chosen areas in the TEM image containing ∼200 nanoparticles each. An energy dispersive X-ray spectroscopy (EDX) analyzer attached to the TEM operating in the scanning transmission electron microscopy (STEM) mode was used to analyze the element distributions in the core−shell, hollow, and cage-bell structured nanoparticles. The electron beam was only 0.7 nm in diameter, capable of providing a high-resolution analysis. UV−visible spectra of the core−shell nanoparticle solution before and after the BSPP treatment were collected on a Shimadzu UV-2450 spectrophotometer. X-ray photoelectron spectroscopy (XPS) was conducted on a VG ESCALAB MKII spectrometer. Powder X-ray diffraction (XRD) patterns were recorded on a Rigaku D/Max-3B diffractometer, using Cu K_α radiation (λ = 1.54056 Å). Sample preparation for XPS and XRD analysis began with concentrating 5 mL of the toluene solution of the metal nanoparticles to 0.5 mL using flowing Ar. Ten milliliters of methanol was then added to precipitate the metal nanoparticles. The nanoparticles were then recovered by centrifugation and washed with methanol several times to remove nonspecifically bound oleylamine. The nanoparticles were then dried at room temperature in vacuum.

2.10. Electrochemical Measurements. Electrochemical measurements were carried out in a standard three-electrode cell, which was connected to a PGSTAT 30 potentiostat. A leak-free Ag/AgCl (saturated with KCl) electrode was used as the reference. The counter electrode was a platinum mesh (1 × 1 cm^2) attached to a platinum wire.

For the loading of the catalyst on Vulcan XC-72 carbon support, a calculated amount of carbon powder was added to the toluene solution of CBS Pt−Ru nanoparticles. After stirring the mixture for 24 h, the CBS Pt−Ru nanoparticles/C (∼20 wt % Pt on carbon support) were collected by centrifugation and washed 3 times with methanol. They were then dried at room temperature in vacuum.

A thin layer of Nafion-impregnated catalyst cast on a vitreous carbon disk was used as the working electrode. Ten milligrams of the CBS Pt−Ru nanomaterials/C was ultrasonically dispersed in 10 mL of aqueous solution containing 4 mL of ethanol and 0.1 mL of the Nafion solution. A calculated volume of the ink was dispensed onto the 5 mm glassy carbon disk electrode to produce a nominal catalyst loading of 20 $\mu g\ cm^{-2}$ (Pt basis). The carbon electrode was then dried in a stream of warm air at 70 °C for 1 h.

A solution of up to 1 M methanol in 0.1 M $HClO_4$ was used for testing the methanol tolerance of the CBS Pt−Ru nanoparticles. The rotation rate of the glass carbon rotating disk electrode (RDE) was 1600 rpm. Negative-going linear sweep voltammograms were recorded from 1 to 0 V at 20 $mV{\cdot}s^{-1}$ at room temperature in the presence of bubbling ultrapure oxygen to maintain a saturated oxygen atmosphere near the working electrode. Current densities were all based on the geometric area (0.196 cm^2) of the glassy carbon electrode.

For comparison, the catalytic activity of a commercial Pt/C catalyst for ORR in 0.1 M $HClO_4$ in the presence of 0.1 M methanol was also evaluated. The commercial Pt/C catalyst was a E-TEK catalyst with 20 wt % Pt nanoparticles (3.2 nm) on Vulcan XC-72 carbon support.

3. RESULTS AND DISCUSSION

We discovered recently that Ag could diffuse out from the core or the inner shell of Ag-containing single or double shell core−shell metal nanoparticles. We will use core−shell Ag−Pt nanoparticles to illustrate this interesting diffusion phenomenon. The TEM images in Figure 1a,b show the initial uniform core−shell Ag−Pt nanoparticles. After storage in toluene for 7 months at room temperature, Ag diffused out from the interior of the core−shell Ag−Pt nanoparticles and TEM showed a product very different from the original nanoparticles (Figure 1c,a): there was increasing presence of isolated Ag nanoparticles and hollow Pt nanoparticles in a mixture of nanoparticles. The high-resolution TEM (HRTEM) image of Figure 1d reveals the structures of the isolated Ag and hollow Pt nanoparticles: two different sets of lattice fringes with separations of 0.236 and 0.228 nm, corresponding well with the {111} planes of face-centered cubic (fcc) Ag and Pt, were found in the solid and hollow nanoparticles, respectively. Two more examples of the inside-out diffusion of Ag may be given. They occurred in core−shell Ag−Ru and core−shell Ag−Rh nanoparticles and are illustrated in Supporting Information Figures S7 and S8, as seen in Part III of Supporting Information (SI).

The inside-out diffusion of Ag was promoted by the structure of the Ag seeds. Figure S1a,b (SI Part I) are the TEM and HRTEM images of Ag nanoparticles synthesized in oleylamine at 150 °C, which were used as seeds in the preparation of core−shell Ag-M nanoparticles. These Ag seeds were ∼9 nm multiply twinned decahedral nanoparticles.[45] The twinned structure had a

dx.doi.org/10.1021/ja302518n | J. Am. Chem. Soc. XXXX, XXX, XXX−XXX

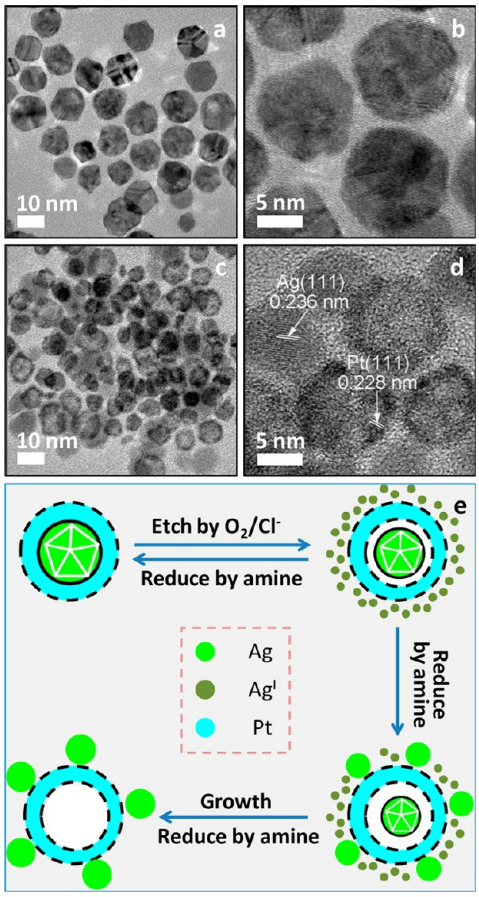

Figure 1. Inside-out diffusion of Ag in core–shell Ag–Pt nanoparticles: (a) TEM and (b) HRTEM images of starting core–shell Ag–Pt nanoparticles; (c) TEM and (d) HRTEM images of core–shell Ag–Pt nanoparticles after aging in toluene for 7 months at room temperature; (e) schematic illustration of the mechanism for the inside-out diffusion of Ag in core–shell Ag–Pt nanoparticles.

strong influence on the stability of the Ag nanoparticles and the overlaid Pt shell. Generally, decahedral particles are mosaic structures consisting of five single crystal tetrahedrons oriented radially about a central axis so that all five tetrahedrons share a common edge in the center, and each tetrahedron has two sides in contact with its neighbors. However, this model is not a space filling one. Since the angle between two {111} planes of a tetrahedron is theoretically 70.53°, five tetrahedrons with adjoining {111} planes will leave a gap of 7.35°. To make up for this difference, significant lattice distortions and defects must occur.[46] These imperfections in the Ag seed nanoparticles were disruptive to the epitaxial deposition of Pt atoms on the Ag seeds, resulting in roughness and discontinuity in the Pt shell subsequently formed. The twinned Ag nanoparticles were also inherently unstable and could slowly be etched by dissolved O_2 and Cl^- dissociated from the Pt precursor. The crystallographic defects in the twinned particles were the active sites for the oxidative dissolution of the nanoparticles. The Ag^I ions released by the O_2/Cl^- etching of twinned Ag nanoparticles could be re-reduced by excess oleylamine in the solution to single crystalline Ag nanoparticles. In principle, the transformation from twinned to single crystalline particles is reversible since O_2/Cl^- etching should also operate on single crystalline Ag nanoparticles. However, as pointed out by Xia and co-workers,[46] single crystalline nanoparticles are less soluble and would continue to grow slowly even in the presence of etchant at the expense of the twinned nanoparticles. Thus, the inside-out diffusion of Ag in core–shell Ag–Pt nanoparticles can be rationalized by the scheme shown in Figure 1e. Because of the concentration gradient between the interior of the core–shell particles and the surrounding solution, the Ag^I ions generated from the O_2/Cl^- etching of twinned Ag seeds diffused out through the discontinuous Pt shell, and were reduced by oleylamine to form isolated single crystalline Ag nanoparticles in the colloidal solution. With the progress of time, the core–shell Ag–Pt nanoparticles would eventually disappear due to the etching and outward diffusion of Ag to leave behind a physical mixture of hollow Pt nanoparticles and single crystalline Ag nanoparticles. Oleylamine was an indispensable multifunctional agent in this case: It was simultaneously a particle stabilizing agent and the reducing agent for the etched Ag ions. Without it, the nucleation and growth of isolated single crystal Ag nanoparticles from dissolved Ag twined particles would not be possible.

The scheme in Figure S9a (SI Part IV) may be used to generate hollow metal nanoparticles by the inside-out diffusion phenomenon of Ag in core–shell nanoparticles. In this protocol, the preparation of core–shell Ag–M nanoparticles is an important step preceding the fabrication of hollow noble metal nanoparticles. Figure S4 (SI Part II) shows the TEM, HRTEM, and scanning TEM (STEM) images of core–shell Ag–Ru, Ag–Rh, Ag–Os, Ag–Ir, and Ag–Pt nanoparticles prepared by the seed-mediated growth method. The formation of core–shell nanoparticles was first suggested by brightness contrast (SI Figure S4a–q) and then confirmed by energy-dispersive X-ray (EDX, SI Figure S4d–t) analyses of arbitrarily chosen single particles in the high-angle annular dark-field scanning TEM mode. As indicated in SI Figure S4d–t, the Ru, Rh, Os, Ir, and Pt signals were present throughout the particle, whereas the Ag signal was detected only in the core region (~9 nm).

However, Figure 1 and SI Figure S7 and S8 also show that the inside-out diffusion of Ag could take months to complete under normal circumstances. This process could however be accelerated by introducing a chemical reagent BSPP, which binds strongly with Ag as Ag^I–BSPP coordination complexes to drive the outward diffusion of Ag in the core–shell nanoparticles,[47,48] enabling the completion of the inside-out diffusion of Ag in a much shorter time frame of 24–28 h (with agitation) after mixing the core–shell Ag–M organosol with an aqueous BSPP solution. The BSPP–Ag^I coordination compounds are water-soluble and their continuous formation left behind an organosol of hollow noble metal nanoparticles, shown by TEM (Figure 2) as an increase in the image contrast between the core and shell regions, and the development of visible discontinuity in the metal shell. The removal of Ag was confirmed by EDX analysis of the final products. As shown in Figure 2c,f,i,l,o, Ag signal was not detected in the core–shell nanoparticles after BSPP treatment. For the core–shell Ag–Pt nanoparticles, the broad absorption in the visible light region due to the surface plasmon resonance of Ag nanoparticles also disappeared after the BSPP treatment (SI Figure S10), corroborating the elimination of the Ag cores from the core–shell Ag–Pt nanoparticles. The powder X-ray diffraction (XRD) patterns (SI Figure S11) of the remaining hollow nanoparticles could be indexed to face-centered cubic (fcc) Rh, Ir, or Pt and hexagonal Ru and Os.[49] The only exception was Pd where nanoparticles with hollow interiors could not be formed this way. The reduction of a Pd precursor in the presence of Ag nanoparticle seeds could not form core–shell nanoparticles; Ag–Pd alloy nanoparticles

dx.doi.org/10.1021/ja302518n | J. Am. Chem. Soc. XXXX, XXX, XXX–XXX

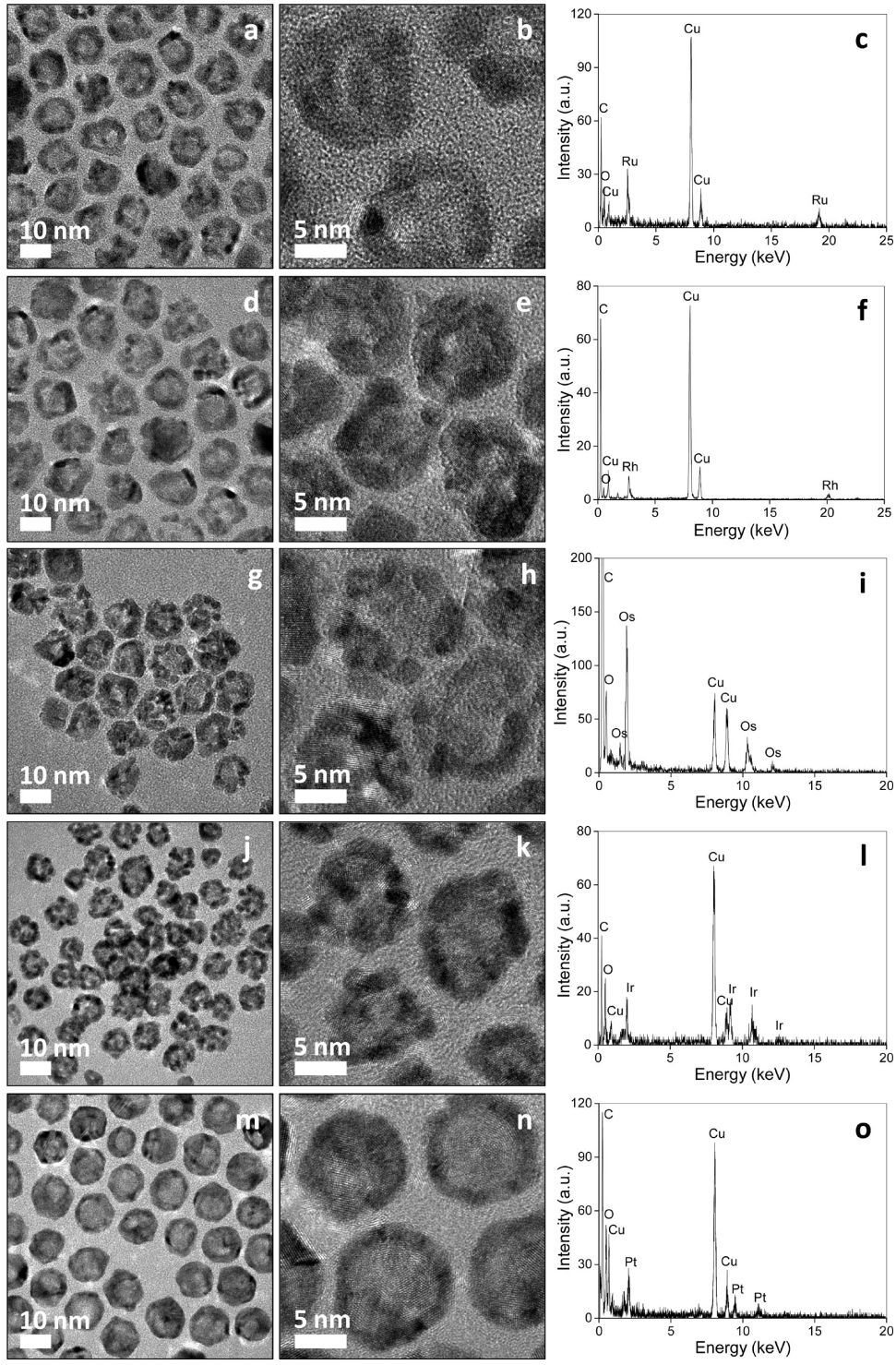

Figure 2. Hollow structured monometallic nanomaterials: (a, d, g, j, and m) TEM images, (b, e, h, k, and n) HRTEM images, and (c, f, i, l, and o) EDX analyses of hollow (a–c) Ru, (d–f) Rh, (g–i) Os, (j–l) Ir, and (m–o) Pt nanoparticles.

(SI Figure S6) were the product instead. HRTEM imaging showed excellent atomic ordering within each particle (SI Figure S6b) indicating no lattice mismatches. The uniform contrast throughout the particle is further proof that mixing of the metallic components occurred at the atomic level. EDX analysis of an arbitrary single particle in the STEM mode (SI Figure S6d) also produced an uniform distribution of Ag and Pd signals across the entire Ag–Pd nanoparticle. The formation of Ag–Pd alloy nanoparticles in organic solution here is similar to the formation of Ag–Au or Ag–Pd alloy nanoparticles by the replacement reaction between Ag nanoparticles and Au or Pd precursors in aqueous solution.[50] Alloying rather than a core–shell construction was caused by the rapid interdiffusion of Ag and Pd atoms at an elevated synthesis temperature.

With a slight modification, the protocol can be used to synthesize hollow alloy nanoparticles (SI Figure S9b). In this case, co-reduction in the presence of preformed Ag seeds involves two or more shell precursor metals in order to form an

dx.doi.org/10.1021/ja302518n | J. Am. Chem. Soc. XXXX, XXX, XXX–XXX

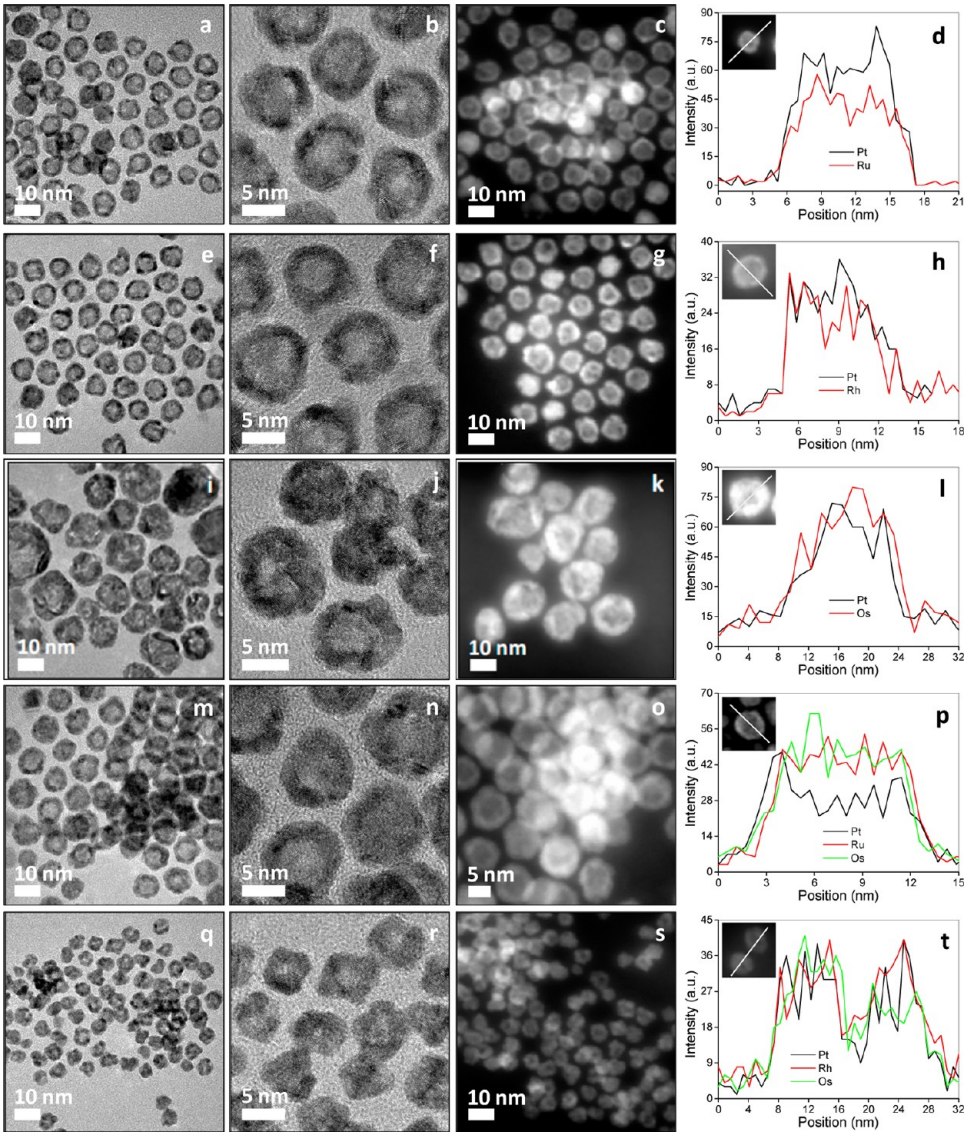

Figure 3. Hollow structured alloy nanoparticles: (a, e, i, m, and q) TEM images, (b, f, j, n, and r) HRTEM images, (c, g, k, o, and s) STEM images, and (d, h, l, p, and t) element profiles of hollow (a–d) PtRu alloy, (e–h) PtRh alloy, (i–l) PtOs alloy, (m–p) PtRuOs alloy, and (q–t) PtRhOs alloy nanoparticles.

alloy shell on the Ag core. The second step remains the same—removal of the Ag core by BSPP treatment. SI Figure S5 shows the TEM, HRTEM, and STEM images of core–shell Ag–PtRu, Ag–PtRh, Ag–PtOs, Ag–PtRuOs, and Ag–PtRhOs nanoparticles prepared in this study. The formation of Ag_{core}–$alloy_{shell}$ nanoparticles was again confirmed by EDX analysis of single particles in the STEM mode. As shown in SI Figure S5d–t, the Ag signal of Ag in all types of core–shell particles was confined to the ~9 nm core region, whereas the Pt and Ru in Ag–PtRu; Pt and Rh in Ag–PtRh; Pt and Os in Ag–PtOs; Pt, Ru, and Os for Ag–PtRuOs; and Pt, Rh, and Os for Ag–PtRhOs were uniformly distributed throughout the nanoparticles. EDX analysis in the STEM mode of core–shell Ag–PtRu, Ag–PtRh, Ag–PtOs, Ag–PtRuOs, and Ag–PtRhOs after the BPSS treatment (Figure 3d–t), on the other hand, confirmed the complete removal of the Ag component, indicating the successful generation of hollow PtRu, PtRh, PtOs, PtRuOs, and PtRhOs alloy nanoparticles. TEM, HRTEM, and STEM images of the hollow nanoparticles are given in Figure 3. The particle size and morphology were virtually unchanged by the BSPP treatment, suggesting that the removal of the Ag core from the core–shell nanoparticles did not cause the collapse of the particle geometry.

It should be mentioned that the aqueous phase after the BSPP treatment, which contained the coordinating compounds formed by BSPP and Ag^I ions, is not a chemical waste. These BSPP–Ag^I coordinating compounds were used to produce monodisperse silver chalcogenide nanocrystals in aqueous solution by reactions with Na_2S, Na_2Se, or Na_2Te at room or elevated temperatures (SI Part V). The TEM and HRTEM images of the Ag_2S, Ag_2Se, and Ag_2Te nanocrystals produced are shown in SI Figure S12. XRD patterns (SI Figure S13) indicate that the Ag_2S and Ag_2Te nanocrystals were monoclinic and the Ag_2Se nanocrystals were orthorhombic. These silver chalcogenide nanocrystals could be further used to generate semiconductor-metal nanocomposites for efficiently catalyzing methanol oxidation at room temperature.[51]

The protocol can be further modified to synthesize noble metal nanoparticles with a cage-bell structure. The cage-bell structure in this work refers to a movable core enclosed by a shell with nanochannels. In principle, the core and shell components

dx.doi.org/10.1021/ja302518n | J. Am. Chem. Soc. XXXX, XXX, XXX–XXX

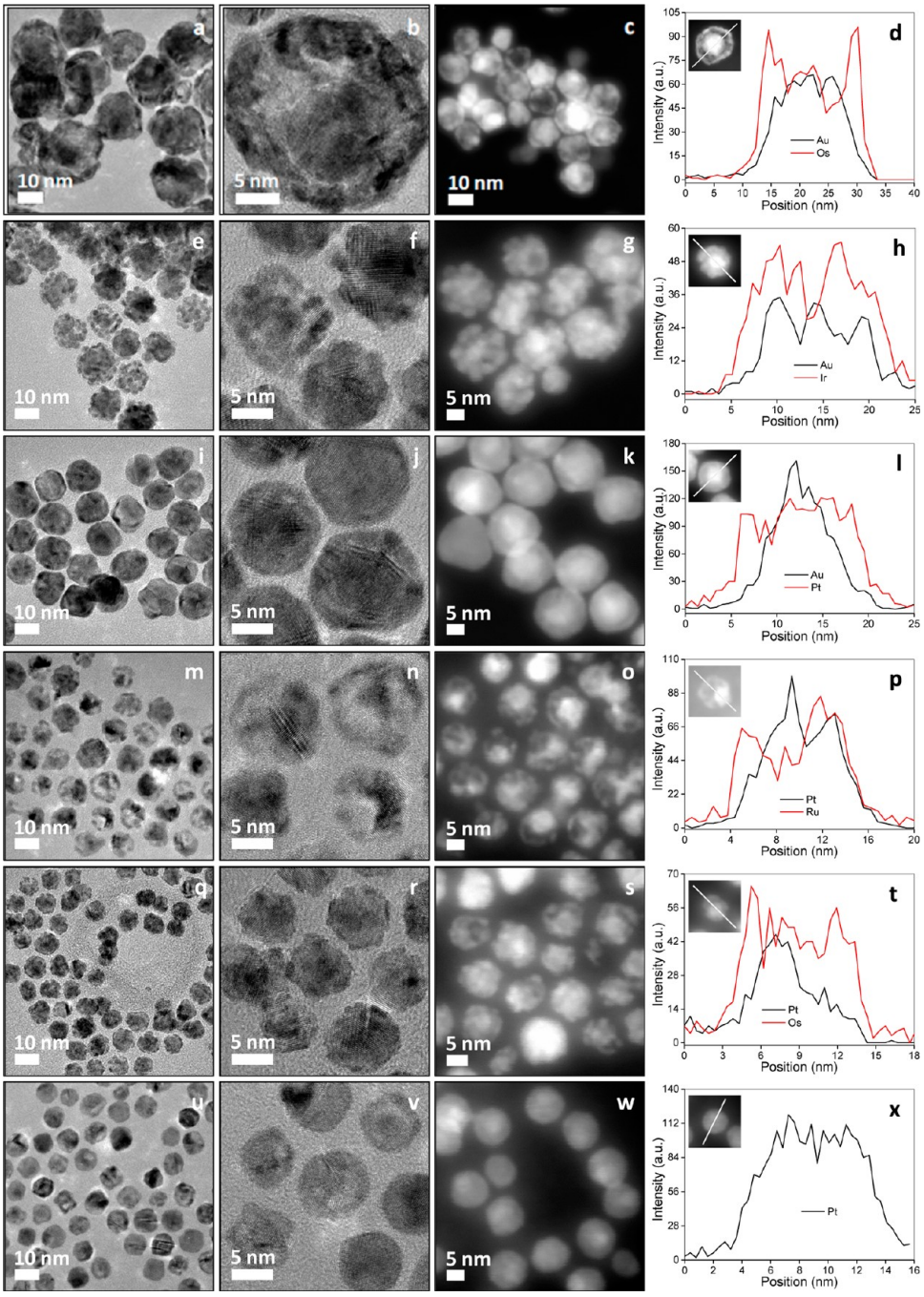

Figure 4. Cage-bell structured (CBS) metal nanomaterials: (a, e, i, m, q, and u) TEM images, (b, f, j, n, r, and v) HRTEM images, (c, g, k, o, s, and w) STEM images, and (d, h, l, p, t, and x) element profiles of (a–d) CBS Au–Os, (e–h) CBS Au–Ir, (i–l) CBS Au–Pt, (m–p) CBS Pt–Ru, (q–t) CBS Pt–Os, and (u–x) CBS Pt–Pt nanoparticles.

may be made of metals or alloys. In the modification illustrated in SI Figure S16, the formation of core–shell–shell M_A–Ag–M_B nanoparticles, in which the inner Ag shell serves as the sacrificial component, is most critical. In the current study, Au and Pt were chosen as the core component (M_A), with Ru, Os, Ir, Pt and alloy PtRh as the outermost shell component (M_B). The syntheses and characterizations of 13 nm Au and 4 nm Pt seed nanoparticles are described in Experimental Section. The successful preparation of the Au and Pt seeds was confirmed by X-ray photoelectron spectroscopy (XPS) (SI Figure S3): a doublet in the XPS spectrum of Au at 83.6 and 87.3 eV assignable to Au at the zero valence state,[52] and two pairs of doublets in the XPS spectrum of Pt. The more intense doublet at 70.8 and 74.1 eV are characteristic of Pt in the zero valence state. The second and weaker doublet at 71.2 and 74.5 eV, with binding energies 1.4 eV higher than those of the zerovalent Pt, may be assigned to PtO.[52] It should be mentioned that a small amount of $AgNO_3$ was used in the synthesis of Pt nanospheres, without which Pt nanotetrapods were formed instead (SI Figure S2).

The procedures in SI Figure S16 were then used to form the CBS nanoparticles. The seed nanoparticles (M_A, Au and Pt) were overlaid with Ag first, followed by the growth of another metal (M_B) shell to form M_A–Ag–M_B nanoparticles with the requisite core–shell–shell structure. Electron microscopy images and the

dx.doi.org/10.1021/ja302518n | J. Am. Chem. Soc. XXXX, XXX, XXX–XXX

results of STEM-EDX analysis of core−shell−shell Au−Ag−Os, Au−Ag−Ir, Au−Ag−Pt, Pt−Ag−Ru, Pt−Ag−Os, Pt−Ag−Ir, Pt−Ag−Pt, and Pt−Ag−PtRh nanoparticles are given in SI Figures S14 and S15, respectively. The core−shell−shell structure was confirmed by the element profiles in SI Figure S14d−l and Figure S15d−t, which show different distributions for different metals across the particle. After BSPP treatment, the inner Ag layer was removed from the M_A−Ag−M_B nanoparticles, leaving behind Au−Os, Au−Ir, Au−Pt, Pt−Ru, Pt−Os, Pt−Ir, Pt−Pt, and Pt−PtRh nanoparticles with the cage bell structure. SI Figure S17 shows the UV−visible spectra in each stage of the preparation of CBS Au−Pt and Pt−Ru nanoparticles, where changes in optical properties after the BSPP treatment may be used an indirect evidence for the elimination of the inner Ag shell from the core−shell−shell M_A−Ag−M_B nanoparticles. More direct evidence was provided by the disappearance of Ag signal in the EDX analysis of core−shell−shell M_A−Ag−M_B after the BSPP treatment (Figure 4d−x and SI Figure S18d−h). Electron microscopy images (Figure 4 and SI Figure S18) show the preservation of the size and morphology of the core−shell−shell nanoparticles in the CBS nanoparticles. The void space between the core and the outer shell regions, formed upon the elimination of the Ag inner shell by BSPP, is discernible by the strong brightness contrast in TEM, HRTEM, and STEM images.

Most of the materials in this work are valuable and important catalytic metals (Pd, Pt, Rh, Ru, PtRh, PtRu, etc); thus, one would expect the hollow and CBS metal nanoparticles to yield significant applications for catalysis due to their advantage of low density, which translated to a higher surface area and would be beneficial to the catalytic reaction.

An unique application was raised by the CBS nanoparticles prepared in this work. The anode and cathode catalysts of current DMFCs are commonly based on Pt. These catalysts are not selective to methanol oxidation reaction (MOR) or oxygen reduction reaction (ORR) and hence any methanol crossover from the anode to the cathode through the proton exchange membrane (PEM) can be oxidized by the cathode catalyst. This results in the creation of a mixed potential at the cathode which degrades the fuel cell performance.[53−55] We discovered that the CBS Pt−Ru nanoparticles have none of the failing of common Pt-based catalysts, and are effectively methanol tolerant in oxygen reduction. As proof, Figure 5a shows the polarization curves of ORR on CBS Pt−Ru nanoparticles in the presence of different methanol concentrations. Even with the presence of methanol in concentrations as high as 1.0 M in the electrolyte, the catalytic reduction of oxygen on the CBS Pt−Ru nanoparticles was hardly affected, demonstrating the effective inhibition of methanol oxidation on the CBS Pt−Ru nanoparticles. For comparison, oxygen reduction on a commercial E-Tek Pt/C catalyst (3−5 nm nanoparticles on carbon powder, SI Figure S19) with and without methanol was also measured (Figure 5b). The ORR polarization curve in this case was clearly affected even at a low methanol concentration of 0.1 M: a valley was formed at the potential for methanol oxidation. In the CBS Pt−Ru catalyst, the catalytically active metal, that is, Pt, is located in the core region shielded by a porous Ru shell. Reactants must diffuse through the porous shell of the CBS nanoparticles to access the active core for catalysis to occur. In this case, the selectivity for ORR may be caused by the porous shell permitting only the passage of small molecule reactants. The situation is depicted by the scheme in Figure 5c. Methanol and oxygen must diffuse into the CBS nanoparticle interior through the porous Ru shell for MOR and ORR to occur. However, a methanol

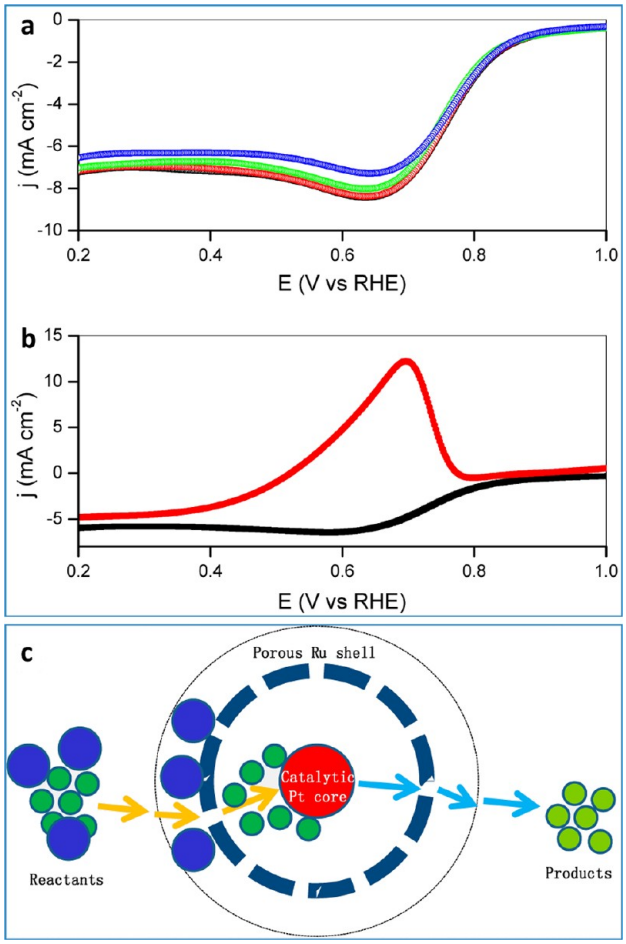

Figure 5. Inhibition of methanol oxidation by CBS Pt−Ru nanoparticles: (a) polarization curves of ORR on CBS Pt−Ru nanoparticles in the presence of (black) 0.0 M methanol, (red) 0.1 M methanol, (green) 0.5 M methanol, and (blue) 1.0 M methanol; (b) polarization curves of ORR on commercial Pt/C catalyst in the presence of (black) 0.0 M methanol and (red) 0.1 M methanol; (c) schematic illustration of the differential diffusion and reaction of reactants in CBS Pt−Ru nanoparticles.

molecule is larger than an oxygen molecule (the diameters of methanol and oxygen molecules are 0.44 and 0.34 nm, respectively). Hence, the diffusion of O_2 is faster than the diffusion of methanol in CBS Pt−Ru nanoparticles, rendering the oxidation of methanol on CBS Pt−Ru a noncompetitive event. By tailoring the structures (e.g., the size of Pt core and the porosity of Ru shell) of the CBS nanoparticles, one would expect the ORR catalytic activity and methanol-tolerant property of CBS Pt−Ru nanoparticles could be further enhanced.

4. CONCLUSION

In summary, we have demonstrated a facile general strategy for the synthesis of noble metal nanoparticles with hollow or cage-bell structures based on the inside-out diffusion of Ag in precursor core−shell composite metal nanoparticles. A selective BSPP treatment was used to accelerate the inside-out diffusion of Ag. The synthesis was carried out at room temperature. The synthesis byproduct of Ag(I)−BSPP complexes could be used for the preparation of silver chalcogenide nanocrystals. The recycling of silver minimizes the environmental footprint and also improves the overall economics of the process. As an unique property, CBS Pt−Ru nanoparticles displayed excellent methanol

dx.doi.org/10.1021/ja302518n | J. Am. Chem. Soc. XXXX, XXX, XXX−XXX

tolerance for ORR at the cathode of the direct methanol fuel cell. The good selectivity is created by the diffusion-limited design, rather than the intrinsic properties of the catalytic metals.

■ ASSOCIATED CONTENT

Supporting Information

XPS studies, UV−visible spectra, XRD patterns, schematic illustrations, additional TEM, HRTEM, STEM images and element profiles for the characterization of the nanostructures in this study. This material is available free of charge via the Internet at http://pubs.acs.org.

■ AUTHOR INFORMATION

Corresponding Authors

*Fax: (+65) 6779 1936; Email: cheleejy@nus.edu.sg (JYL)

*Fax: (+86) 10-8254 4814; Email: jyang@mail.ipe.ac.cn (JY)

Notes

The authors declare no competing financial interest.

■ ACKNOWLEDGMENTS

This work was funded by the National Natural Science Foundation of China (Project No.: 21173226), 100 Talents Program of the Chinese Academy of Sciences, and the Institute of Bioengineering and Nanotechnology (Biomedical Research Council, Agency for Science, Technology and Research, Singapore).

■ REFERENCES

(1) Kim, S.-W.; Kim, M.; Lee, W. Y.; Hyeon, T. *J. Am. Chem. Soc.* **2002**, *124*, 7642−7643.
(2) Li, Y.; Zhou, P.; Dai, Z.; Hu, Z.; Sun, P.; Bao, J. *New J. Chem.* **2006**, *30*, 832−837.
(3) Cheng, F.; Ma, H.; Li, Y.; Chen, J. *Inorg. Chem.* **2007**, *46*, 788−794.
(4) Liang, H.-P.; Zhang, H.-M.; Hu, J.-S.; Guo, Y.-G.; Wan, L.-J.; Bai, C.-L. *Angew. Chem., Int. Ed.* **2004**, *43*, 1540−1543.
(5) Lee, J.; Park, J. C.; Song, H. *Adv. Mater.* **2008**, *20*, 1523−1528.
(6) Gough, D. V.; Wolosiuk, A.; Braun, P. V. *Nano Lett.* **2009**, *9*, 1994−1998.
(7) Liu, J.; Qiao, S. Z.; Hartono, S. B.; Lu, G. Q. *Angew. Chem., Int. Ed.* **2010**, *49*, 4981−4985.
(8) Gao, J.; Liang, G.; Zhang, B.; Kuang, Y.; Zhang, X.; Xu, B. *J. Am. Chem. Soc.* **2007**, *129*, 1428−1433.
(9) Zhao, W.; Chen, H.; Li, Y.; Li, L.; Lang, M.; Shi, J. *Adv. Funct. Mater.* **2008**, *18*, 2780−2788.
(10) Zhu, Y.; Ikoma, T.; Hanagata, N.; Kaskel, S. *Small* **2010**, *6*, 471−478.
(11) Zhang, W.-M.; Hu, J.-S.; Guo, Y.-G.; Zheng, S.-F.; Zhong, L.-S.; Song, W.-G.; Wan, L.-J. *Adv. Mater.* **2008**, *20*, 1160−1165.
(12) Lou, X. W.; Li, C. M.; Archer, L. A. *Adv. Mater.* **2009**, *21*, 2536−2539.
(13) Chen, J. S.; Li, C. M.; Zhou, W. W.; Yan, Q. Y.; Archer, L. A.; Lou, X. W. *Nanoscale* **2009**, *1*, 280−285.
(14) Chen, J. S.; Luan, D.; Li, C. M.; Boey, F. Y. C.; Qiao, S.; Lou, X. W. *Chem. Commun.* **2010**, *46*, 8252−8254.
(15) Chen, J. S.; Wang, Z.; Dong, X. C.; Chen, P.; Lou, X. W. *Nanoscale* **2011**, *3*, 2158−2161.
(16) Li, H.; Bian, Z.; Zhu, J.; Zhang, D.; Li, G.; Huo, Y.; Li, H.; Lu, Y. *J. Am. Chem. Soc.* **2007**, *129*, 8406−8407.
(17) Benabid, F.; Couny, F.; Knight, J. C.; Birks, T. A.; Russell, P. J. *Nature* **2005**, *434*, 488−491.
(18) Kamata, K.; Lu, Y.; Xia, Y. *J. Am. Chem. Soc.* **2003**, *125*, 2384−2385.
(19) Bai, F.; Sun, Z.; Wu, H.; Haddad, R. E.; Xiao, X.; Fan, H. *Nano Lett.* **2011**, *11*, 3759−3762.
(20) Caruso, F.; Caruso, R. A.; Möhwald, H. *Science* **1998**, *282*, 1111−1114.
(21) Caruso, F.; Shi, X.; Caruso, R. A.; Susha, A. *Adv. Mater.* **2001**, *13*, 740−744.
(22) Yang, Z.; Niu, Z.; Lu, Y.; Hu, Z.; Han, C. C. *Agnew. Chem., Int. Ed* **2003**, *42*, 1943−1945.
(23) Lou, X. W.; Yuan, C.; Archer, L. A. *Small* **2007**, *3*, 261−265.
(24) Peng, Z.; Wu, J.; Yang, H. *Chem. Mater.* **2010**, *22*, 1098−1106.
(25) Wang, Z.; Luan, D.; Boey, F. Y. C.; Lou, X. W. *J. Am. Chem. Soc.* **2011**, *133*, 4738−4741.
(26) Lai, X.; Li, J.; Korgel, B. A.; Dong, Z.; Li, Z.; Su, F.; Du, J.; Wang, D. *Angew. Chem., Int. Ed.* **2011**, *50*, 2738−2741.
(27) Schmidt, H. T.; Ostafin, A. E. *Adv. Mater.* **2002**, *14*, 532−535.
(28) Hubert, D. H. W.; Jung, M.; German, A. L. *Adv. Mater.* **2000**, *12*, 1291−1294.
(29) Gao, X.; Zhang, J.; Zhang, L. *Adv. Mater.* **2002**, *14*, 290−293.
(30) Nakashima, T.; Kimizuka, N. *J. Am. Chem. Soc.* **2003**, *125*, 6386−6387.
(31) Qi, L.; Li, J.; Ma, J. *Adv. Mater.* **2002**, *14*, 300−303.
(32) Zhang, D.; Qi, L.; Ma, J.; Cheng, H. *Adv. Mater.* **2002**, *14*, 1499−1502.
(33) Wong, M. S.; Cha, J. N.; Choi, K.-S.; Deming, T. J.; Stucky, G. D. *Nano Lett.* **2002**, *2*, 583−587.
(34) Lou, X. W.; Archer, L. A.; Yang, Z. *Adv. Mater.* **2008**, *20*, 3987−4019.
(35) Zhao, Y.; Jiang, L. *Adv. Mater.* **2009**, *21*, 3621−3638.
(36) Liu, J.; Qiao, S. Z.; Chen, J. S.; Lou, X. W.; Xing, X.; Lu, G. Q. *Chem. Commun.* **2011**, *47*, 12578−12591.
(37) Chen, H. M.; Liu, R.-S.; Lo, M.-Y.; Chang, S.-C.; Tsai, L.-D.; Peng, Y.-M.; Lee, J.-F. *J. Phys. Chem. C* **2008**, *112*, 7522−7526.
(38) Skrabalak, S. E.; Chen, J.; Sun, Y.; Lu, X.; Au, L.; Cobley, C. M.; Xia, Y. *Acc. Chem. Res.* **2008**, *41*, 1587−1595.
(39) Yin, Y.; Rioux, R. M.; Erdonmez, C. K.; Hughes, S.; Somorjai, G. A.; Alivisatos, P. A. *Science* **2004**, *304*, 711−714.
(40) Zeng, H. C. *J. Mater. Chem.* **2006**, *16*, 649−662.
(41) Zeng, H. C. *Curr. Nanosci.* **2007**, *3*, 177−181.
(42) Caruso, F. *Chem.—Eur. J.* **2000**, *6*, 413−419.
(43) Wu, X.-J.; Xu, D. *J. Am. Chem. Soc.* **2009**, *131*, 2774−2775.
(44) Li, G.; Shi, Q.; Yuan, S. J.; Neoh, K. G.; Kang, E. T.; Yang, X. *Chem. Mater.* **2010**, *22*, 1309−1317.
(45) Tsuji, M.; Ogino, M.; Matsuo, R.; Kumagae, H.; Hikino, S.; Kim, T.; Yoon, S.-H. *Cryst. Growth Des.* **2010**, *10*, 296−301.
(46) Wiley, B.; Herricks, T.; Sun, Y.; Xia, Y. *Nano Lett.* **2004**, *4*, 1733−1739.
(47) Yang, J.; Lee, J. Y.; Too, H. P.; Valiyaveettil, S. *J. Phys. Chem. B* **2006**, *110*, 125−129.
(48) Tan, Y.-N.; Yang, J.; Lee, J. Y.; Wang, D. I. C. *J. Phys. Chem. C* **2007**, *111*, 14084−14090.
(49) McClune, W. F., Eds.; *Powder Diffraction File Alphabetical Index Inorganic Phase*; JCPDS: Swarthmore, PA, 1980.
(50) Zhang, Q.; Lee, J. Y.; Yang, J.; Boothroyd, C.; Zhang, J. *Nanotechnology* **2007**, *18*, 245605/1−245605/8.
(51) Yang, J.; Ying, J. Y. *Angew. Chem., Int. Ed.* **2011**, *50*, 4637−4643.
(52) Wagner, C. D.; Naumkin, A. V.; Kraut-Vass, A.; Allison, J. W.; Powell, C. J.; Rumble, J. R. *NIST Standard Reference Database 20*, version 3.2 (web version).
(53) Gasteiger, H. A.; Markovic, N.; Ross, P. N.; Cairns, E. J. *J. Phys. Chem.* **1993**, *97*, 12020−12029.
(54) Wang, J. M.; Brankovic, S. R.; Zhu, Y.; Hanson, J. C.; Adzic, R. R. *J. Electrochem. Soc.* **2003**, *150*, A1108−A1117.
(55) Antolini, E.; Salgado, J. R. C.; Gonzalez, E. R. *J. Electroanal. Chem.* **2005**, *580*, 145−154.